Implementation and Performance Evaluation of 100- kHz, Soft-Switched Bidirectional PFC/Inverter with Silicon MOSFETs

Brian T. Irving, Yungtaek Jang, and Milan M. Jovanović
Delta Power Electronics Laboratory
Delta Products Corporation
Research Triangle Park, NC, USA

***Abstract*— In this paper, the performance of a bidirectional ac/dc converter which utilizes silicon MOSFETs and operates in continuous-conduction mode (CCM) with 100-kHz switching frequency is evaluated. The converter is implemented with an active snubber that virtually eliminates losses related to the reverse-recovery charge of the body diodes of Si MOSFET switches and also provides for their zero-voltage switching (ZVS). The circuit operation was verified with a 3.3 kW PFC/inverter experimental prototype designed for 230-V_{RMS} nominal ac voltage and 400-V dc voltage. The measured circuit efficiency in both directions is greater than 97.9% at loads greater than 45%.**

Keywords—Bidirectional, Soft-switching ac-dc

I. INTRODUCTION

Bidirectional converters are increasingly being used in power systems with energy-storage capabilities, such as micro-grid and automotive applications where they are employed to condition charging and discharging of energy-storage devices such as batteries and super-capacitors. As illustrated in Fig. 1, in bidirectional ac-dc converters the front-end power-factor correction (PFC) /inverter is implemented with the controllable-bridge circuit [1]. To avoid excessive body-diode reverse-recovery losses [2], the bridge switches whose body diodes do not have significant reverse-recovery charge, such as insulated gate bipolar transistors (IGBTs) or recently available wide-bandgap-semiconductor switches such as gallium nitride (GaN) and silicon carbide (SiC) switches, must be selected. Generally, implementations with IGBTs [3] are limited to relatively low switching frequencies due to the turn-off switching loss of the IGBT, whereas, SiC and GaN devices, which virtually do not exhibit reverse-recovery charge and can efficiently operate at very high switching frequencies [4]-[11], are not presently cost effective.

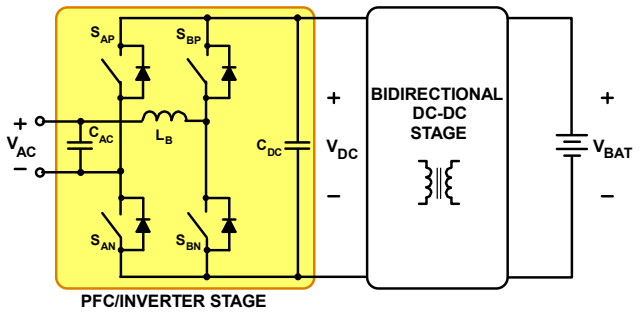

Fig. 1 Block diagram of typical bidirectional power supply.

To efficiently and reliably employ silicon MOSFET switches in the bidirectional PFC/inverter front end operating at high switching frequencies, it is necessary to reduce the reverse-recovery charge of their body diodes by providing soft switching. Soft switching can be achieved either by operating the switches in discontinuous conduction mode (DCM) [12] or by adding a snubber circuit when operating in continuous conduction mode (CCM) [13]-[20].

In this paper, the active snubber introduced by X. Yuan and I. Barbi in [14] was used to implement and evaluate a 100-kHz soft-switched PFC/inverter that employs Si MOSFET switches. Originally, in [14], the active snubber was applied to implement a 6.5-kHz IGBT-based inverter by providing zero-voltage switching (ZVS) of IGBTs so that the lossless capacitive turn-off snubber could be used to reduce their turn-off loss. In the PFC/inverter implementation described in this paper, the same snubber is primarily employed to enable the use of MOSFET switches by reducing their switching loss by virtually eliminating the reverse-recovery charge of their body diodes as well as to provide ZVS. The performance of this implementation was evaluated on an experimental 100-kHz, 3.3-kW prototype. The prototype was designed to operate from a 400 V dc input and deliver a regulated 230 V sinusoidal ac output in inverter mode and from 180-264-V ac line and deliver 400-V dc output in rectifier mode. The measured efficiency in both directions is greater than 97.9% at loads greater than 45%.

II. SOFT-SWITCHED BIDIRECTIONAL PFC/INVERTER

The bidirectional PFC/Inverter with the active snubber proposed in [14] is shown in Fig. 2. As highlighted in Fig. 2, the active snubber consists of snubber inductor L_S, snubber transformer T, snubber switches S_{BPSNB} , S_{BNSNB}, and snubber diodes D_{CP}, D_{CN}, D_{DP}, and D_{DN} connected as the full-bridge rectifier.

Generally, in the circuit in Fig. 2, the pair of switches in the same bridge leg are switched in a complementary fashion. Specifically, the S_{AP}-S_{AN} pair is switched at the line frequency, whereas the S_{BP}-S_{BN} pair at the switching frequency. Active

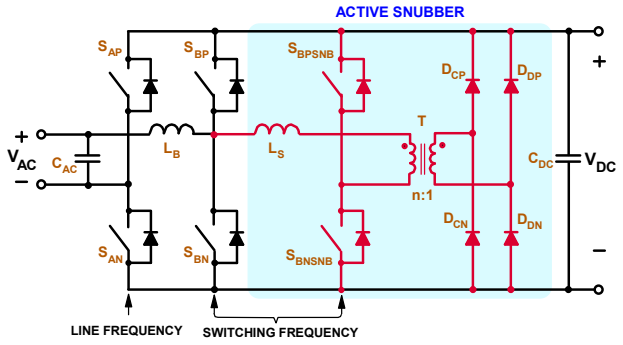

Fig. 2 Bidirectional PFC/inverter with soft switching active snubber.

snubber switches S_{BPSNB} and S_{BNSNB} also operate with the switching frequency but are not complimentary.

To facilitate the explanation of the circuit operation, Fig. 3 shows a simplified circuit diagram where a single switching cycle is analyzed during a positive half-line cycle in rectifier mode. Inductor L_B, which operates in continuous-conduction mode (CCM) is replaced with an ideal current source by assuming that its inductance is large so that during a switching cycle the current through it does not change significantly. In addition, energy-storage capacitor C_{DC} is modeled by voltage source V_{DC} by assuming that the value of C_B is large enough so that the voltage ripple across the capacitor is small in comparison to its dc voltage. Line-frequency switches S_{AP}, S_{AN} and snubber switches S_{BPSNB}, S_{BNSNB} are considered to be ideal (i.e., have zero on resistance, and no terminal capacitances), whereas main switches S_{BP} and S_{BN} are modeled with output capacitances and body diodes which exhibits reverse-recovery characteristics. In this analysis, snubber inductor L_S represents the sum of a discrete inductor and the leakage inductance of snubber transformer T. As a result, snubber transformer T is modeled with its magnetizing inductance L_M and turns ratio n. Finally, snubber diodes D_{CP}, D_{CN}, D_{DP}, and D_{DN} are modeled as ideal diodes without junction capacitance.

To further facilitate the explanation of circuit operation, Fig. 4 shows the key topological stages of the circuit shown in Fig. 2 during a switching cycle, whereas Fig. 5 shows its key waveforms. The reference directions of currents and voltages plotted in Fig. 5 are shown in Fig. 3.

It can be seen from the timing diagrams (a) and (b) in Fig. 5 that during positive line cycle low-frequency switch S_{AP} is off

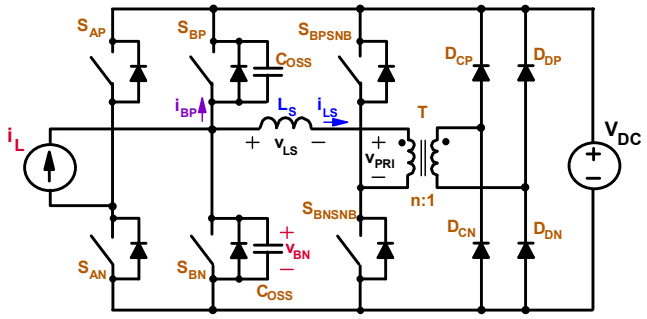

Fig. 3 Simplified circuit diagram of bidirectional PFC/inverter with soft switching active snubber.

whereas switch S_{AN} is on. It can also be seen from the timing diagrams (c)-(f) in Fig. 5 that the turn-on instances of main switches S_{BP} and S_{BN} are delayed by short delay time T_{DELAY} with respect to the turn-on instances of their corresponding snubber switches.

Prior to the turn on of snubber switch S_{BNSNB}, i.e., at $t < t_0$, all switches are open, and inductor current i_L flows through the body diode of main switch S_{BP}, voltage source V_{DC}, and low-frequency switch S_{AN}, as shown in Fig. 4(a). At $t = t_0$, snubber switch S_{BNSNB} is turned on. If turns ratio n less than unity is selected, snubber diodes D_{CP} and D_{CN} are forward biased so that V_{DC} is imposed across the secondary winding of the transformer developing primary-winding voltage $V_{PRI} = nV_{DC}$. Because in this topological stage, shown in Fig. 4(b), constant voltage V_{DC}- nV_{DC} is applied across snubber inductor L_S, snubber inductor current i_{LS} starts linearly increasing causing the current in the body-diode of S_{BP} to decrease at the same rate, i.e.,

$$\frac{di_{LS}}{dt} = -\frac{(1-n)V_{DC}}{L_S}. \qquad (1)$$

For a given turns ratio n, the turn-off rate of the body-diode can be controlled by the proper selection of inductance value L_S. To virtually eliminate reverse-recovery charge of body diodes of today's MOSFETs, the body-diode-current turn-off rate should be kept around 100 A/μs.

As illustrated in Fig. 5, snubber inductor current i_{LS} continues to increase until it reaches the level of boost inductor current i_L and the body-diode current of switch S_{BP} reduces to zero. After the body-diode of switch S_{BP} stops conducting at $t = t_1$, snubber inductor L_S begins to resonant with output capacitance C_{OSS} of main switches S_{BP} and S_{BN}, as shown in Fig. 4(c). To resonate drain-source voltage V_{BN} down to zero and achieve ZVS, turns ratio n should be chosen less than 0.5, [21]. As illustrated in Fig. 5, drain-source voltage V_{BN} reaches zero at $t = t_2$.

For proper operation of the circuit, it is necessary to provide delay between the turn on of snubber switch S_{BPSNB} and the turn on of main switch S_{BP}. This delay must be long enough to enable main-switch drain-source voltage V_{BN} to resonate down to zero. Minimum delay time T_{DELAY}^{min} is given by

$$T_{DELAY}^{min} = t_2 - t_0 = \frac{i_L L_S}{V_{DC}(1-n)} + \pi\sqrt{L_S(2C_{OSS})}, \qquad (2)$$

where the first term represents time interval $t_1 - t_0$, i.e., the time the snubber inductor current i_{LS} takes to increase from zero to boost-inductor current i_L, and the second term represents time interval $t_2 - t_1$, i.e., a half period of the resonance between snubber inductor L_S and the parallel connection of output capacitances C_{OSS} of main switches S_{BN} and S_{BP}.

After drain-source voltage V_{BN} of switch S_{BN} reaches zero at $t = t_2$, snubber inductor current i_{LS} continues to flow through the body-diode of switch S_{BN}, as shown in Fig. 4(d). Because in this topological stage primary voltage $V_{PRI} = nV_{DC}$ is connected in negative direction across snubber inductor L_S, current i_{LS} begins decreasing linearly toward zero.

In Fig. 5, switch S_{BN} is turned on with ZVS at $t = t_3$. The topological stage after the turn on of switch S_{BN} is shown in Fig. 4(e). During this stage, snubber inductor current i_{LS} that is

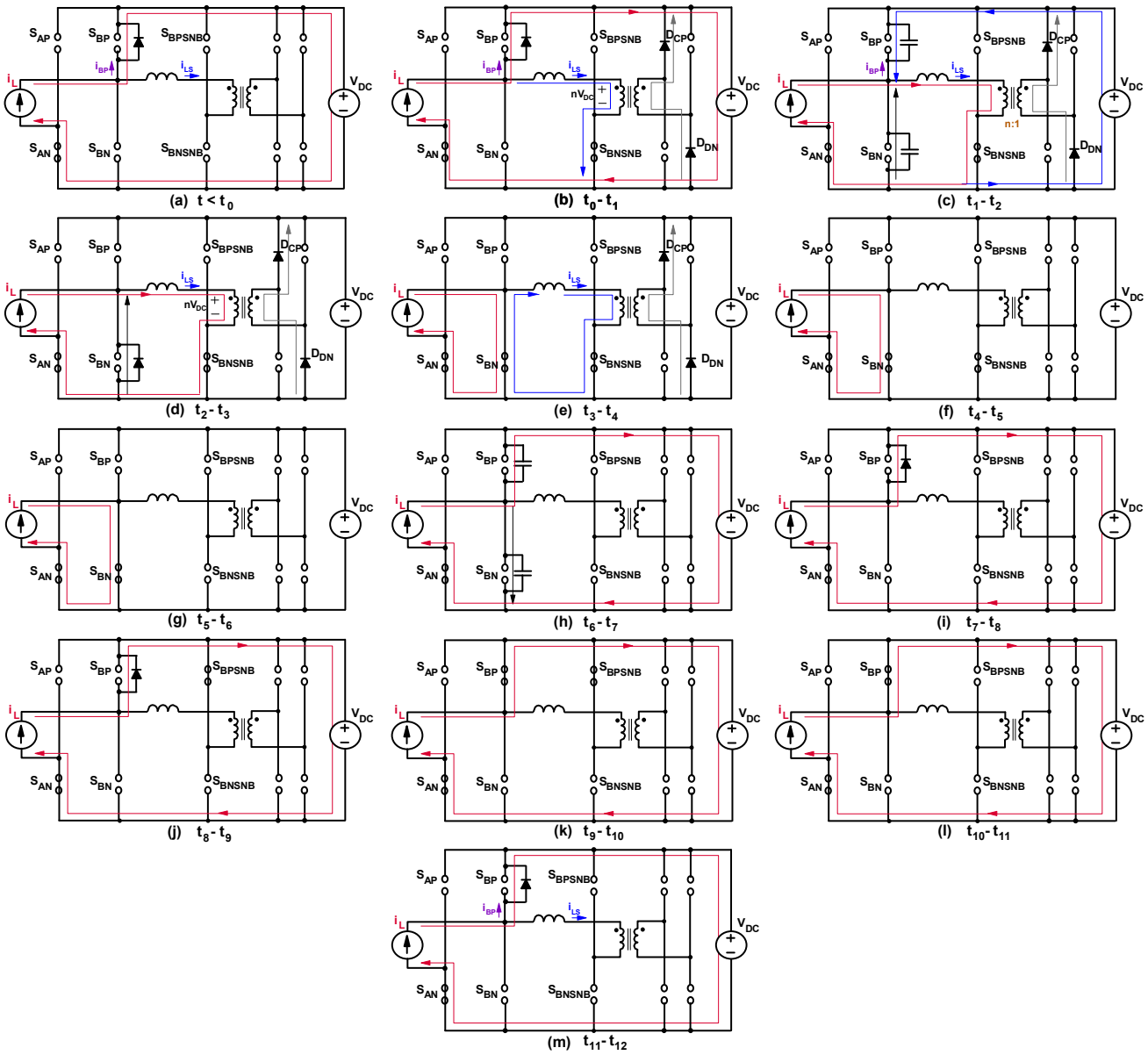

Fig. 4 Topological stages during a switching period of bidirectional PFC/inverter with soft switching active snubber during positive half period.

diverted from the body-diode to the channel of switch S_{BN} continues to linearly decrease. When it reaches zero at $t = t_4$, the circuit enters the topological stage shown in Fig. 4(f). In this stage, snubber inductor current i_{LS} stays at zero because secondary-side snubber rectifiers prevent it from flowing in the negative direction. To achieve zero-current-switching of snubber switch S_{BNSNB}, the switch should be turned off after $t = t_4$. In Fig. 5, switch S_{BNSNB} is turned off at $t = t_5$. During the topological stage t_5–t_6, snubber inductor current i_{LS} continues to be zero, whereas boost inductor current i_L continues to flow through closed switches S_{AN} and S_{BN}, as shown in Fig. 4(g). When switch S_{BN} is turned off at $t = t_6$, boost inductor current i_L starts commutating from switch S_{BN} to switch S_{BP} by resonantly charging output capacitance of switch S_{BN} and discharging output capacitance of switch S_{BP}, as shown in Fig. 4(h). After output capacitance of switch S_{BP} is fully discharged at $t = t_7$, boost-inductor current i_L continues to flow through the body-diode of switch S_{BP}, as shown in Fig. 4(i).

As shown in Fig. 5, upper snubber switch S_{BPSNB} is turned on at $t = t_8$, as originally proposed in [14]. However, as shown in Fig. 4(j), the turning on of switch S_{BPSNB} has no effect since the boost-inductor current is positive (in phase with input voltage) and flows through the body diode of upper switch S_{BP}. If the boost-inductor current were negative, i.e., flowing through the body diode of lower switch S_{BN}, the turning on of switch S_{BPSNB} would generate snubber-inductor current i_{LS}, i.e., activate the snubber to provide soft switching of body diode of S_{BN}. Therefore, since in the PFC mode that is illustrated in Figs. 4 and 5 the input current and voltage are in phase, the snubber switch S_{BPSNB} does not need to be turned on at $t = t_8$. However,

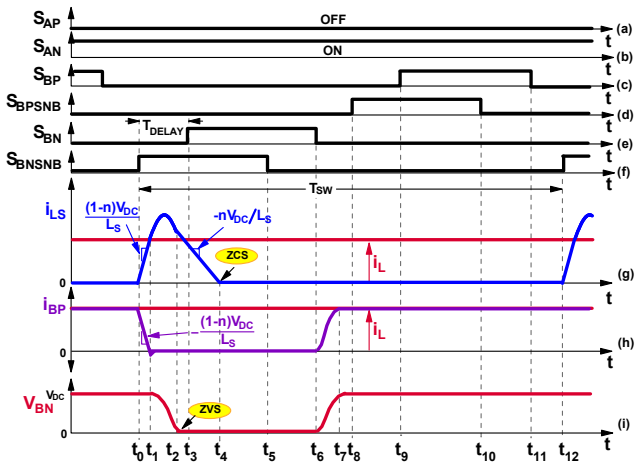

Fig. 5 Key switching waveforms of PFC/inverter with soft-switching active snubber during positive half line period.

in inverter mode switch S_{BPSNB} must be operated because for reactive loads the current and voltage are not in phase.

As shown in in Fig. 5, switch S_{BP} is operated as a synchronous-rectifier (SR) switch to reduce the conduction loss of its body diode. It is turned on with ZVS on at $t = t_9$ and turned off at $t = t_{11}$. During its on time, boost-inductor current i_L is flowing through the switch channel instead the body diode, as illustrated in Figs. 4(k)-(m). For proper operation of the circuit, upper snubber switch S_{BPSNB} must be turned off before upper main switch S_{BP} is turned off. In Fig. 5, switch S_{BP} is turned off at $t = t_{11}$. Finally, the new switching cycle starts when snubber switch S_{BNSNB} is turned on again at $t = t_{12}$.

The operation during the negative half of input voltage is exactly the same except that snubber switch S_{BPSNB} is used to control the snubber.

Finally, it should be noted that because of the ZCS of snubber switches S_{BPSNB} and S_{BNSNB}, IGBTs (Insulated Gate Bipolar Transistors) are the most suitable devices for their implementation. Either MOSFETs or IGBTs are suitable for low-frequency switches S_{AP} and S_{AN}.

III. Experimental Results

The performance of the active snubber was evaluated on the 3.3 kW, 100-kHz experimental prototype shown in Fig. 6. The prototype was designed to operate with 180-264-V_{RMS} ac-input voltage range and deliver 400-V dc output in rectifier mode and provide regulated 230-V_{RMS} / 60 Hz ac output from a 400-V input in inverter mode.

The maximum voltage stress of all semiconductor devices is determined by dc-side voltage V_{DC}=400 V. To handle 28-A peak current, which occurs at full load and low line, IPW65R041CFD MOSFET (V_{DSS} = 650 V, I_{D25} = 68.5 A, R_{DSON} = 41 mΩ) from Infineon were used for main bridge switches S_{AP}, S_{AN}, S_{BP}, and S_{BN}. Snubber switches S_{BPSNB} and S_{BNSNB} that need to handle a peak current of approximately 30 A were implemented by IKW40N65F5 IGBT (V_{DSS} = 650 V, I_{D25} = 40 A, V_{CESAT} = 2.1 V) from Infineon. Finally, VS-4EGH06-M3 fast-recovery diodes (V_R = 600 V, $I_{F(AVG)}$ = 4 A, V_F = 1.2 V) from Vishay were used for snubber diodes D_{CP}, D_{CN}, D_{DP}, and D_{DN} whose peak current is approximately 11 A.

To obtain the desired inductance of boost inductor L_B of approximately 200 µH at full load, the boost inductor was built using two toroidal 77192-A7 cores from Magnetics with 34 turns of AWG #12 magnet wire wound around both cores together.

Snubber transformer T was built using Ferroxcube ferrite core PQ35/35 3F3 with an air gap of 0.3 mm. Both primary and secondary windings were wound with Litz wire (N_P = 14 turns and 0.1mm x 180 strands, N_S=39 turns and 0.1 mm x 120 strands) which results in magnetizing inductance L_M = 100 µH. A 5-W, 12-kΩ resistor was placed across the secondary winding to damp parasitic ringing.

Snubber inductor L_S was built using TDK ferrite core PQ26/25Z-12 PC40 with an air gap of 2.3 mm wound with fiveturns of 0.1 mm x 300 strands Litz wire to give a value of 2.3 µH.

Additional 100 nF capacitors were connected across drain-source of line-frequency MOSFETs S_{AP} and S_{AN} to decrease

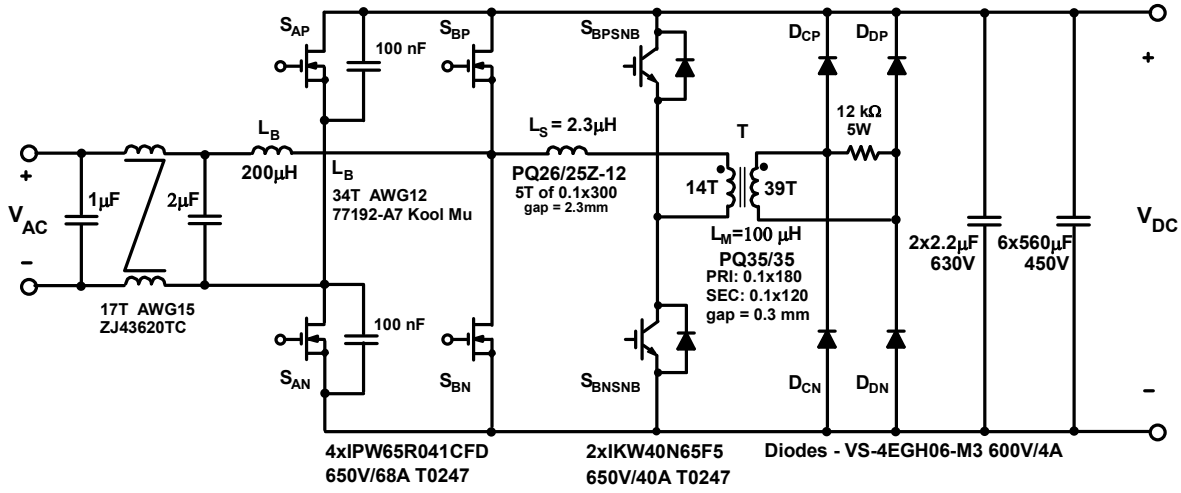

Fig. 6 Experimental prototype circuit of bidirectional PFC/inverter with soft switching active snubber.

parasitic ringing around the zero crossing of voltage V_{AC}.

Constant time delay T_{DELAY}=300 ns was set over the ac-line cycle. Also, on time of snubber switches S_{BPSNB} and S_{BNSNB} was set constant and equal to 1.6 µs. Generally, soft-switching was achieved over the entire line cycle except at the zero crossing of voltage V_{AC} when the active snubber was disabled.

Figure 7 shows an oscillogram of key waveforms in the experimental converter in rectifier mode when it delivers full power at nominal input voltage V_{AC} = 230 V_{RMS}. The waveforms are taken around the positive peak of line voltage. As can be seen in Fig. 7, gate-source voltage of lower switch S_{BN} increases smoothly without noticeable Miller effect, which implies ZVS. In addition, it is shown that snubber switch S_{BNSNB} turns off when snubber inductor current i_{LS} is zero, i.e., operates with ZCS.

Figures 8 and 9 show oscillograms of key line-frequency waveforms at nominal line voltage V_{AC} = 230 V_{RMS} and full load in rectifier and inverter mode, respectively. In rectifier mode, input current i_{AC} shown in Fig. 8 has a power factor of 0.99 and a current Total Harmonic Distortion (THD) less than 1%. For resistive load in inverter mode, shown in Fig, 9, ac output voltage V_{AC} has a power factor of 1 and a voltage THD less than 1%. Figure 10 shows an oscillogram of key line-frequency waveforms in inverter mode with inductive load. The inductive load consists of a 30-mH inductor connected in series with a

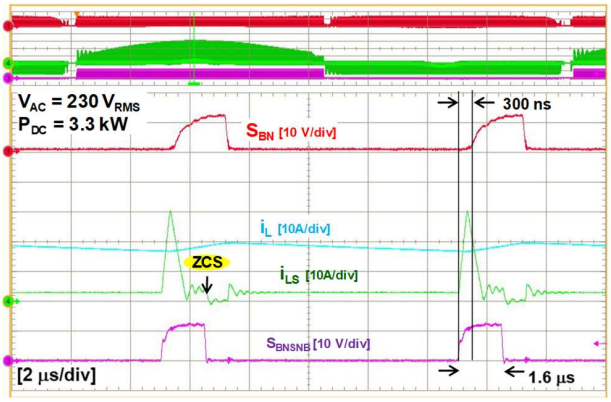

Fig. 7 Measured waveforms of the experimental prototype in rectifier mode at V_{AC} = 230 V_{RMS}, V_{DC} = 400 V, P_{DC} = 3.3 kW.

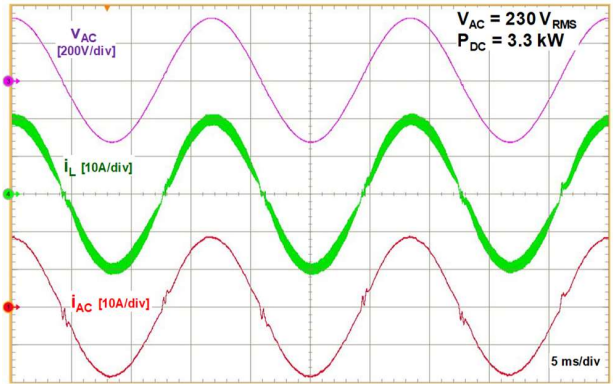

Fig. 8 Measured line waveforms of the experimental prototype in rectifier mode at V_{AC} = 230 V_{RMS}, V_{DC} = 400 V, P_{DC} = 3.3 kW.

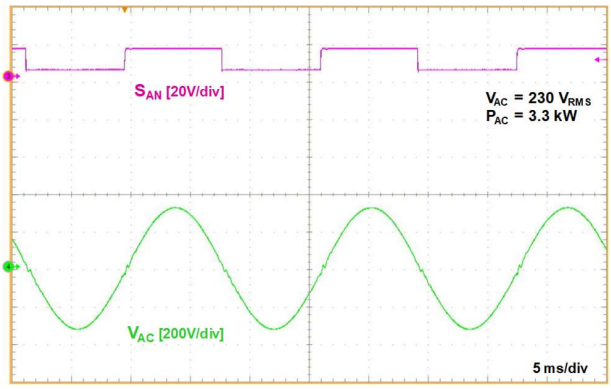

Fig. 9 Measured line waveforms of the experimental prototype in inverter mode with resistive load at V_{AC} = 230 V_{RMS}, V_{DC} = 400 V, P_{DC} = 3.3 kW.

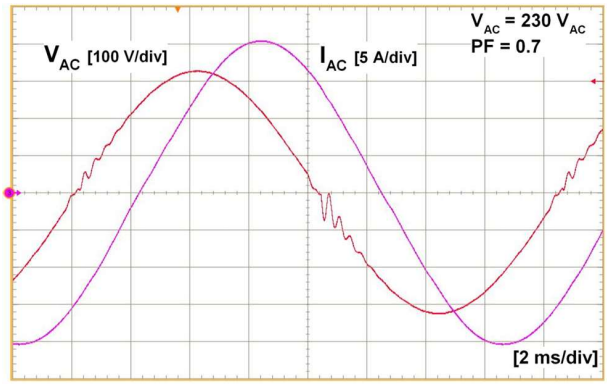

Fig. 10 Measured line waveforms of the experimental prototype in inverter mode with inductive load at V_{AC} = 230 V_{RMS} and 3.3 kVA.

12- Ω resistor, resulting in an apparent power of 3.3 kVA and power factor of 0.7. The measured THD of voltage V_{AC} shown in Fig. 10 is less than 1%.

Figure 11 shows the measured resistive-load efficiency of the experimental circuit without soft-switching active snubber (i.e., with hard-switching operation) in both rectifier and inverter mode. Hard-switching operation was limited to below 500 W in

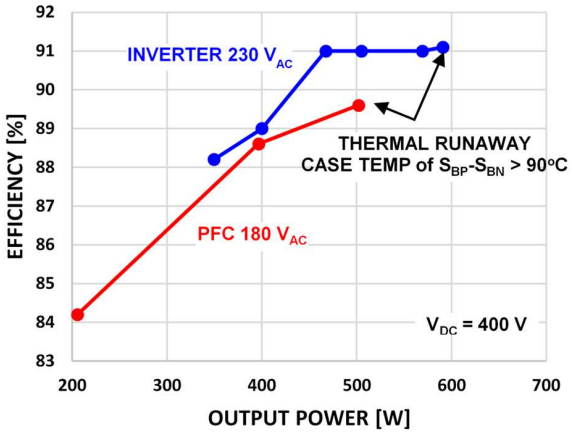

Fig. 11 Measured efficiency of the experimental converter without soft-switching active snubber in both rectifier (in red) and inverter (in blue) mode.

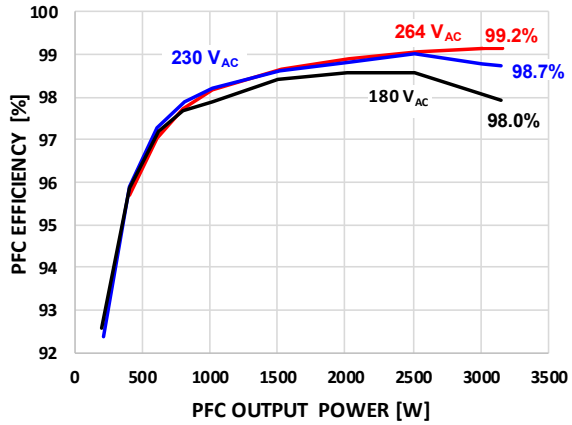

Fig. 12 Measured efficiency of the experimental converter in rectifier mode with soft-switching active snubber.

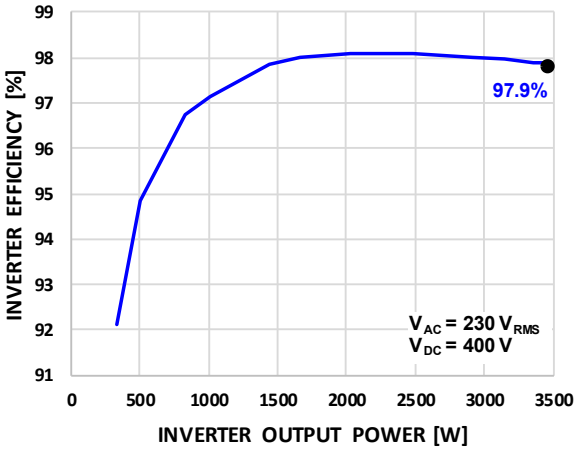

Fig. 13 Measured efficiency of the experimental converter in inverter mode with resistive load and soft-switching active snubber.

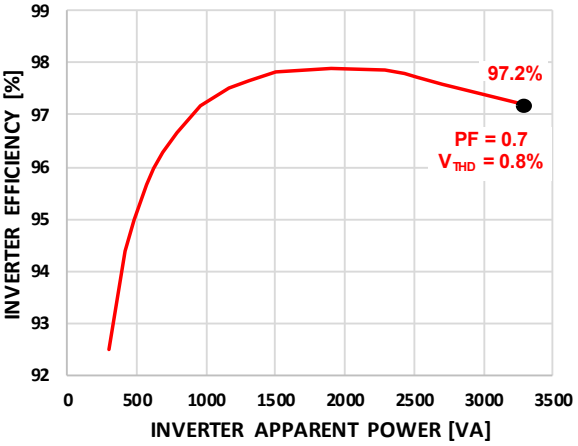

Fig 14 Measured efficiency of the experimental converter in inverter mode with inductive load and soft-switching active snubber.

rectifier mode, and below 600 W in inverter mode due to the excessively high temperature of the main switches S_{BP} and S_{BN}. Both switches had a case temperature exceeding 90°C after several minutes indicating thermal runaway.

Figure 12 shows the measured rectifier-mode efficiency of the experimental circuit with soft-switching active snubber for ac input voltages V_{AC} = 180, 230, and 264 V_{RMS}. The efficiency exceeded 98% at loads greater than 1 kW (>30% load). Main switches S_{BP} and S_{BN} had the highest case temperature of all semiconductor devices at 45°C. Figure 13 shows the measured resistive-load efficiency of the experimental circuit in inverter mode. The efficiency exceeds 97.9% at loads greater than 1.5 kW (>45% load). Temperature of main switches S_{BP} and S_{BN} that is the highest temperature of all semiconductor devices was 46°C. Finally, Fig. 14 shows the measured efficiency of the experimental circuit with soft-switching active snubber in inverter mode with inductive load. The measured full-load efficiency is 97.2%. It should be noted that the efficiency measurements in Figs. 11-14 do not include gate-driver and controller losses, and all measurements were performed at a room temperature of 22°C.

IV. SUMMARY

The performance of the proposed active snubber was evaluated on a 3.3 kW bidirectional ac-dc converter implemented with conventional silicon MOSFET switches and operating with 100 kHz switching frequency. The measured efficiency of the experimental prototype in rectifier mode at nominal input voltage V_{AC}=230 V_{RMS} exceeded 98% above 30% load. In inverter mode, the efficiency was greater than 97.9% above 45% load at 230V_{AC} output.

REFERENCES

[1] J. C. Salmon,"Circuit topologies for PWM boost rectifiers operated from 1-phase and 3-phase ac supplies and using either single or split dc rail voltage outputs,"*in Proc. IEEE Appl. Power Electron. Conf.*, 1995, pp. 473–479.

[2] Y. Khersonsky, M. Robinson, and D. Gutierrez, "New fast recovery diode technology cuts circuit losses, improves reliability," in *Power Convers. Intell. Motion Magazine*, 1992, pp. 16 - 25.

[3] Y.H. Liao, "A novel reduced switching loss bidirectional ac/dc converter pwm strategy with feedforward control for grid-tied microgrid systems", *IEEE Trans. Power Electron.*, vol. 29, no.3, pp. 1500-1513, Mar. 2014.

[4] L. Huber, Y. Jang and M. M. Jovanović, "Performance evaluation of bridgeless pfc boost rectifiers," in *IEEE Trans. Power Electron.,* vol. 23, no. 3, pp. 1381-1390, May 2008.

[5] Y. Tang, W. Ding, and A. Khaligh, "A bridgeless totem-pole interleaved pfc converter for plug-in electric vehicles", *in Proc. IEEE Appl. Power Electron. Conf.*, 2016, pp. 440–445.

[6] L. Zhou, Y. Wu, and U. Mishra, "True-bridgeless totem-pole pfc based on GaN HEMTs", *in Proc. Power Convers. Intell. Motion Conf.*, 2013, pp. 1017-1022.

[7] Z. Ye, A. Agular, Y. Bolurian and B. Daugherty, "GaN fet-based ccm totem-pole bridgeless pfc," *The 23rd TI Power Supply Design Seminar*, 2014.

[8] B. Sun "How to reduce current spikes at ac zero-crossing for totem-pole PFC" *Texas Instruments Analog Applications Journal (AAJ)*, 4Q, 2015, publication slyt650.

[9] F.C. Lee, Q. Li, Z. Liu, Y. Yang, C. Fei, and Mingkai Mu, "Application of GaN devices for 1 kW server power supply with integrated magnetics," *CPSS Trans. Power Electron. Appl.*, vol. 1, no. 1, pp. 3-12, Dec. 2016.

[10] B. Li, F.C. Lee, Q. Li and Z. Liu, "Bi-directional on-board charger architecture and control for achieving ultra-high efficiency with wide battery voltage range", *in Proc. IEEE Appl. Power Electron. Conf.*, 2017, pp. 3688–3694.

[11] Y. Yang, Z. Liu, F.C. Lee, and Q. Li, "Multi-phase coupled and integrated inductors for critical conduction mode totem-pole pfc converter", *in Proc. IEEE Appl. Power Electron. Conf.*, 2017, pp. 1804–1809.

[12] B. Su and Z. Lu, "An interleaved totem-pole boost bridgeless rectifier with reduced reverse-recovery problems for power factor correction", *IEEE Trans. Power Electron.*, vol. 25, no.6, pp. 1406-1415, Jun. 2010.

[13] R. W. De Doncker and J. P. Lyons, "The auxiliary resonant commutated pole inverter," in *Proc. IEEE IAS Annu. Meet. Rec*, 1990, pp. 1228-1235.

[14] X. Yuan and I. Barbi, "Analysis, designing, and experimentation of a transformer-assisted pwm zero-voltage switching pole inverter," *IEEE Trans. Power Electron.*, vol. 15, no.1, pp. 72-82, Jan. 2000.

[15] W. McMurray, "Resonant snubbers with auxiliary switches," *IEEE Trans.Ind. Appl.*, vol. 50, no.3, pp. 1966-1973, May/June 2014.

[16] W. Yu, J. S. Lai, and S. Y. Park, "An improved zero-voltage switching inverter using two coupled magnetics in one resonant pole", *IEEE Trans. Power Electron.*, vol. 25, no.4, pp. 952-961, Apr. 2010.

[17] R. C. Beltrame, J. R. R. Zientarski, M. L. D. S. Martins, J. R. Pinheiro, and H. L. Hey, "Simplified zero-voltage-transition circuits applied to bidirectional poles: concept and synthesis methodology", *IEEE Trans. Power Electron.*, vol. 26, no.6, pp. 1765-1776, Jun. 2011.

[18] J. S. Lai, W. Yu, P. Sun, S. Leslie, B. Arnet, C. Smith, and A. Cogan, "A hybrid-switch-based soft-switching inverter for ultrahigh-efficiency traction motor drives," *IEEE Trans. Ind. Appl.*, vol. 50, no.3, pp. 1966-1973, May/Jun.. 2014.

[19] K. Stengert, "On-board 22 kw faster charger "NLG6"", *IEEE Elect. Vehicle Symp.*, 2013, pp. 1-11.

[20] J. M. A. Myrzik, J. L. Duarte, P. de Haardt, and J. Vissers, "Transformer-assisted pwm zero-voltage switching pole inverter with high output bandwidth applied to linear motor drives," IEEE Industry Appl. Conf., 2002, pp. 2351-2357.

[21] Y. Jang, M.M. Jovanović, K.H. Fang, and Y.M. Chang, "High-power-factor soft-switched boost converter", *IEEE Trans. Power Electron.*, vol. 21, no. 1, pp. 98-104, Jan. 2006.